Research Article

Nano Biomed Eng

Graphene Quantum Dots Incorporated UiO-66-NH$_2$ Based Fluorescent Nanocomposite for Highly Sensitive Detection of Quercetin

Sopan Nangare[1], Sayali Patil[1], Kalyani Chaudhari[1], Zamir Khan[1], Ashwini Patil[2], Pravin Patil[1]✉

[1] Department of Pharmaceutical Chemistry, H. R. Patel Institute of Pharmaceutical Education and Research, Shirpur, India
[2] Department of Microbiology, R. C. Patel Arts, Science and Commerce College, Shirpur, India

✉ Corresponding author. E-mail: rxpatilpravin@yahoo.co.in

Abstract

Quercetin can help with a variety of health problems. Most methods for measuring quercetin in biological fluids are characterized by low sensitivity and selectivity. The employment of metal–organic frameworks in sensor applications with carbon-based materials ushers in a new era. In this study, blue fluorescent graphene quantum dots (GQDs) embedded in a UiO-66-NH$_2$ metal–organic framework-based nanoprobe (GQDs@UiO-66-NH$_2$) were constructed for quercetin sensing. Initially, maize husk was used to produce blue fluorescent GQDs, whereas zirconium tetrachloride and 2-aminoterephthalic acid were used to synthesize extremely luminous UiO-66-NH$_2$. The addition of quercetin to GQDs@UiO-66-NH$_2$ leads to fluorescence dampening due to the adsorption potential of UiO-66-NH$_2$. The complexation of zirconium ions with the 3-OH and 4-C=O functionalities of quercetin resulted in fluorescence quenching. The sensor has a linear concentration range and limit of detection for quercetin of 50–500 and 2.82 ng/mL, respectively. The nanoprobe's usefulness for quercetin detection was then validated by a selectivity investigation in the presence of interfering chemicals. Furthermore, the percentage relative standard deviations were 4.20% and 2.90%, respectively, indicating great stability and repeatability. Fluorescence "Turn-On–Off" nanoprobes provide a simple, quick, sensitive, and selective method for monitoring quercetin.

Keywords: quercetin; graphene quantum dots (GQDs); fluorescence; nanoprobe; metal–organic framework; GQDs@UiO-66 NH$_2$; sensitivity

Introduction

Quercetin is the most important flavonoid in fruits and vegetables [1]. It does not produce in human bodies [2]. Quercetin is widely reported for antioxidant, antiviral, immunomodulation, antitumor [3], and anti-inflammatory [4] applications. The literature claimed that 945 mg/m^2 is the safe dose for quercetin. A high dose of quercetin can produce different several health issues including hypertension, a decline in potassium levels in serum, and emesis [2]. Therefore, accurate measurement of the concentration of quercetin is essential in the biomedical field [3]. Moreover, to measure the bioavailability of quercetin, it is essential for pharmacological response [1]. In general, analysis of quercetin with a simplistic, speedy, highly selective, and sensitive method is a prime necessity [4].

Numerous techniques for determining quercetin have been documented, including high-performance liquid chromatography (HPLC) [1, 5], HPLC-tandem mass spectrometry, ultraviolet (UV)–visible (Vis) spectroscopy [6], gas chromatography (GC)-mass spectrometry (MS) [7], capillary electrophoresis [8, 9], etc. in body fluids including plasma [1, 6], urine[1], etc. Uses of a colorimetric method, chromatographic method, electrophoresis, etc., are suffering from numerous demerits including high cost, being time-consuming, requiring sophisticated instruments, etc [10]. In addition, there are chances of poor sensitivity and selectivity towards the target analyte. Hence, owing to several physical parameters dependency, it resulted in the unsuitability for monitoring of target analyte [7, 9, 11].

Nanomaterial-based recognition has earned tremendous consideration from the research community for the construction of sophisticated biomedical applications such as sensor design [12]. Presently, different types of sensing systems have been revealed for the recognition of quercetin including electrochemical sensors [3, 8], fluorescence base sensors [13], etc. In this shade, nanoflake–nanorod tungsten disulfide [2], gold nanoparticles–graphene composite [11], silica gel-mediated carbon paste electrodes [4], multi-wall carbon nanotubes (MWCNTs) modified glassy carbon electrode (GCE) [14], silver–silica-based polyethylene glycol hybrid nanoparticles [9], carbon nanotube (CNT) modified electrode [7], etc., have been used for monitoring of quercetin in complexed samples. Herein, carbon-based fluorescence sensors have been widely preferred for sensing target analytes owing to their plenty of merits including speedy identification, cost-effectiveness, simplicity, high sensitivity, and selective detection capability [15]. Out of several carbon-based materials, fluorescent graphene quantum dots (GQDs) gained much attention from budding researchers in diverse fields including biosensing, chemical sensing, drug delivery, bioimaging, etc [15, 16]. Principally, it consists of nanometer-sized materials made of single/multi-layered graphenes. It has been divulged that light emission has size-based band gaps [17]. In addition, GQDs offer good biocompatibility, tunable photoluminescence, water-solubility, lower cost, and low toxicity [13, 18]. Different GQDs-based fluorescence sensors have been documented including gold nanoparticle-GQDs-mediated nanozyme [19],

sulfur-doped GQDs [13], MoS_2-CNTs@GONRs/HS-CD/GQDs composite [20], etc. Despite this, there are indeed significant concerns with sensitivity and selectivity toward an intended target in the specimens presented.

Metal–organic frameworks (MOFs) have been used to capture biomarkers [21] and chemical ions [22, 23]. Such nanostructures offer high porosity, larger surface area, surface tunability, etc [24]. Because of their distinct and adaptable features, luminous MOFs have recently been recognized for sensing applications among a plethora of MOFs [25]. Overall, the properties of MOFs that promise luminous inorganic frameworks represent substantial benefits above other conceivable kinds of sensing elements. Furthermore, the logical creation of such structures has emerged as the key objective in the investigation of MOFs as detecting materials [26]. Mainly, zirconium and 2-aminoterphthalic acid (BDC-NH$_2$ or 2-ATA)-mediated UiO-66-NH$_2$ (UiO-66: Universitetet i Oslo) have gained huge consideration from researchers for sensing applications possibly because of their hopeful chemical and physical characteristics [27]. MOFs have several drawbacks, including structural collapse and fluorescence intensity [28]. Several investigations reported the incorporation of GQDs into MOFs for measurement applications wherein GQDs can be uniformly dispersed and distributed in MOFs [17]. The functionality of such GQDs@MOFs-based fluorescent nanosensors is offered in aspects of responsiveness, specificity, measurement speed, etc [29]. Principally, it may be because of the synergistic presentation of GQDs and luminescent MOFs [29, 30]. According to this research, the spongy framework of UiO-66-NH$_2$ may encourage the inclusion of nanosized GQDs, resulting in improved performance [26]. Despite plenty of advancement in sensing quercetin, a highly luminescent GQDs@UiO-66-NH$_2$ nanoprobe is still missing for the detection of quercetin. As a result, GQDs-adorned MOF-based fluorescent nanoprobes might be employed to measure quercetin.

The present study aims to construct a bright blue luminescent GQDs@UiO-66-NH$_2$ based "Turn-Off" nanoprobe for the sensing of quercetin (Fig. 1) with enhanced effectiveness in terms of responsiveness, specificity, detection speed, involved cost, manufacturing, sensing tactic, etc., that contrasted to initially disclosed detectors. Green synthesis of GQDs was obtained from green precursor using
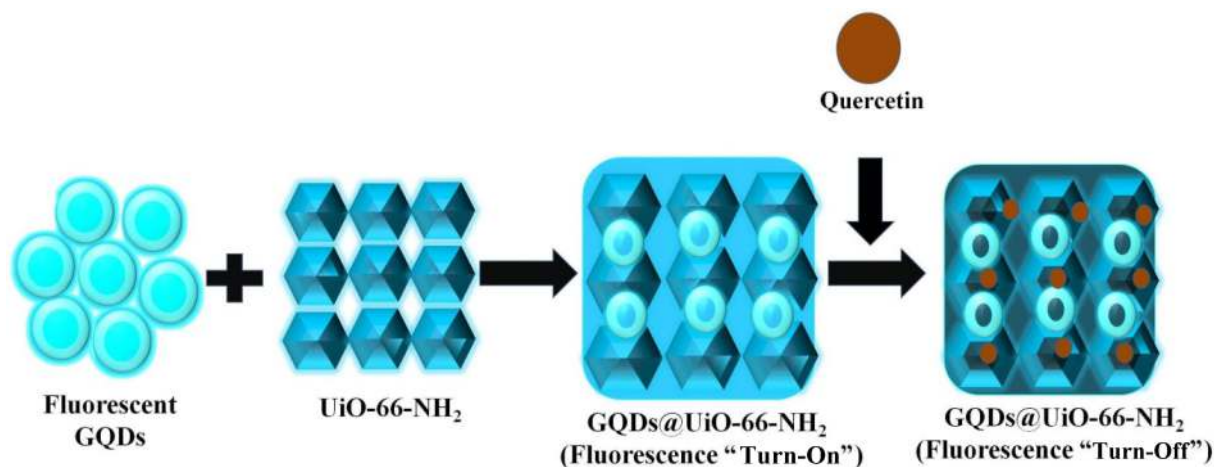
Fig. 1 Freshly manufactured GQDs and UiO-66-NH$_2$ coupled to generate a luminescent "Turn-Off" nanoprobe for the measurement of quercetin.

hydrothermal method, whereas synthesis of fluorescent luminescent UiO-66-NH$_2$ was prepared using 2-ATA as a ligand and zirconium (Zr) as metal ions source. The sensing of quercetin in phosphate buffer (pH=7.4) was studied, whereas selectivity analysis was performed using different interfering substances. As a consequence, the suggested luminescent GQDs@UiO-66-NH$_2$ nanoprobe affords a straightforward, environmentally, cost-effective, quick, highly specific, and delicate function for quercetin identification. As a corollary, this fluorescence detector will enable a different option for monitoring flavonoids in clinical specimens.

Materials and Methods

Materials

For the present study, zirconium tetrachloride (ZrCl$_4$, 98%) was purchased from Chemica-Biochemica reagents, India. 2-Aminoterephthalic acid (2-ATA/BDC-NH$_2$, 99%) was purchased from Sigma Aldrich, India. Loba Chemie, Chemicals, Pvt. Ltd. (Mumbai, India) provided the dimethylformamide (DMF, 99%) and quercetin. Ethanol was purchased from Anil cottage industries, A/31, M.I.D.C., Wardha-442006 (M. S.). Merck Specialties Pvt. Ltd. provided the potassium dihydrogen phosphate (PDP, 99%) and sodium hydroxide (NaOH). Cornhusk was acquired from the Shirpur (Dhule) local market in India. The H. R. Patel Institute of Pharmaceutical Education and Research at Shirpur provided double distilled water (DDW). Each of the chemicals involved in the study was analytical grade and unadulterated and used as a delivered by the supplier.

Methods

Green synthesis of GQDs

In this study, the hydrothermal approach was used to produce exceptionally bright blue fluorescent GQDs from cornhusks (Fig. 2). Initially, obtained 100 g of cornhusk was trimmed into tiny chunks. Then, it was powdered in a laboratory crusher for further use. 50 g of ground husk fibers was then diffused in an ethanol–water combination with a ratio of 20∶40 for 2 days at room temperature to eliminate any pollutants and dust. After a couple of days, the corn husk fibers were withdrawn from the aforesaid mixture and heated for 1 h in a laboratory hot air oven (Bio-Technics, India) at 100 °C before being triturated. Following that, 3 g of fibers was poured into 40 mL of DDW, which was then constantly stirred at 100 r/min for 15 min with a laboratory magnetic stirrer at room temperature. After this, to generate GQDs, the solution was poured into a Teflon-lined autoclave in a stainless-steel hydrothermal vessel and housed in a 160 °C laboratory oven for 12 h [15]. The solution was cooled to room temperature when the hydrothermal phase was accomplished. The color of the solution changed from yellow-white to yellowish-brown during this phase, likely due to the cornhusk. The resulting GQDs were then filtered using 0.22 μm pore size membrane filter paper and freeze-dried (Southern Scientific Lab Instrument, Chennai, India) following the procedure from Ref. [15]. In the first step, green synthesized GQDs were subjected to the primary freezing process wherein concentrated GQDs were made at 30 °C for 12 h using a deep freezer. The frozen GQDs solution was then freez-fried for 24 h at −53 °C and under the pressure
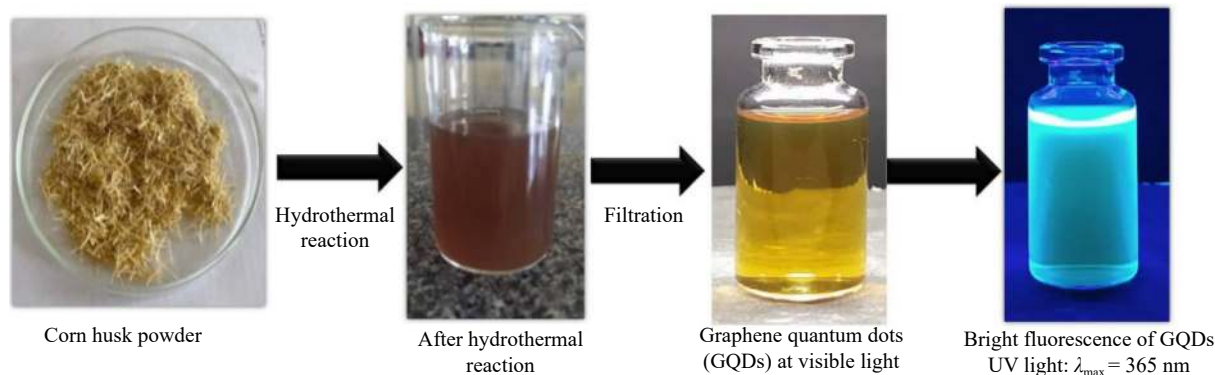
Fig. 2 Synthesis of GQDs from corn husk powder.

of 1.6 Pa. After the primary drying of GQDs, secondary drying was performed to remove the remaining moist content from GQDs powder. Herein, the temperature was maintained at 10 °C for 8 h, and then increased up to 25 °C for 4 h. Subsequently, the temperature continuously rose with a rate of 1 °C/min. To complete the drying phase, the temperature of the cold trap end was tuned to –53 °C. The green-produced GQDs-free dried powder was then tested for several spectroscopic analyses.

Synthesis of MOFs

A formerly published simple methodology was utilized for the production of Uio-66-NH$_2$ with slight modification [31]. First, 0.348 g of ZrCl$_4$ was dissolved in an exact volume of 65 mL of DMF, and then 0.276 g of 2-ATA was added into a solution of ZrCl$_4$, followed by sonication for 20 min at 25 °C. The solution was then placed in a teflon-lined autoclave over 120 °C for 24 h to accomplish the manufacturing of intensely luminous Uio-66-NH$_2$. Thereafter, the autoclaved mixture was treated to cold centrifugation at 20 000 r/min for 25 min at 25 °C (Elteck Overseas Pvt., India) to isolate Uio-66-NH$_2$. At this stage, Uio-66-NH$_2$ was washed with the ethanol, and then again washed with DDW in triplicate to eliminate contaminants. Furthermore, the resulting Uio-66-NH$_2$ was freeze-dried following the earlier described freeze-drying process [15]. To evaluate the effective synthesis of MOF, freeze-dried Uio-66-NH$_2$ was analyzed using several spectroscopic methods.

Fabrication of GQDs@UiO-66-NH$_2$ nanoprobe

Highly luminous GQDs@UiO-66-NH$_2$ nanoprobe was developed using the previously discussed solvothermal approach [30] with slight modification. To begin with, 10 mg of freeze-dried GQDs were transferred to a clean 50-mL volumetric flask

(200 μg/mL), followed by volume adjustment with DDW, and then sonication for 15 min at 30 °C. Later, 2 mg of UiO-66-NH$_2$ powder was poured into a cleansed 10-mL volumetric flask, and the volume was corrected with DDW. Following that, different concentrations of UiO-66-NH$_2$ were prepared to obtain the suitable concentration for the fabrication of a highly fluorescent GQDs@UiO-66-NH$_2$ nanoprobe for sensing quercetin. Herein, an optimum concentration of UiO-66-NH$_2$ was added into the previously prepared GQDs solution and following that, transferred to bath sonication for 1 h at 30 °C. The resulting combination of GQDs and UiO-66-NH$_2$ was then moved to the autoclave and steamed (120 °C over 24 h). The solid phase of the nanosensor was then segregated out from the free form of GQDs employing cold centrifugation around 20 000 r/min for 30 min at 25 °C. Subsequently, washing was performed using DDW in triplicate. Last, the prepared highly luminous GQDs@UiO-66-NH$_2$ nanoprobe was subjected to freeze-drying using the previously reported method and then further used for spectroscopical characterizations and sensing of quercetin.

Characterizations of GQDs, UiO-66-NH$_2$, and GQDs@UiO-66-NH$_2$ nanoprobe

To assure eco-friendly synthesis of GQDs, UiO-66-NH$_2$, and GQDs@UiO-66-NH$_2$ nanoprobe, different characterizing techniques including UV–Vis spectroscopy, UV cabinet study, particle size analysis, Fourier transform infrared spectroscopy (FTIR), zeta potential analysis, fluorescence study using spectrofluorometer, and high-resolution transmission electron microscopy (HR-TEM) were preferred. Initially, synthesized GQDs, UiO-66-NH$_2$, and GQDs@UiO-66-NH$_2$ based nanoprobe were tested for UV–Vis spectrum utilizing a UV–Vis

spectrophotometer (UV 1800 Shimadzu, Japan) employing a quartz cuvette with a wavelength of 200–800 nm. After that, a fluorescent study of synthesized GQDs, UiO-66-NH$_2$, and GQDs@UiO-66 NH$_2$ was performed using a laboratory UV cabinet (Southern Scientific Lab Instrument, Chennai, India). It assists to confirm fluorescence in visible light and at different wavelengths such as λ_{max} = 254 and 365 nm. For the identification of distinct functional groups, the FTIR spectra of GQDs, UiO-66-NH$_2$, and GQDs@UiO-66-NH$_2$ were measured using an FTIR spectrophotometer (IR Affinity-1S Shimadzu). Subsequently, fluorescence tests, such as GQDs, UiO-66-NH$_2$, and GQDs@UiO-66-NH$_2$ nanoprobe, were accomplished using a spectrofluorometer (JASCO International Co., Ltd., Japan). A particle size analyzer (Nanoplus 3 Particulate System, Micromeritics, USA) was performed to validate the particle size, as well as the zeta potential of GQDs, UiO-66-NH$_2$, and GQDs@UiO-66-NH$_2$ nanoprobe, which contributes to evaluate the actual dimensions and durability in a solvent system. Furthermore, HR-TEM (Jeol/JEM 2100; Light source: LaB6 (200 kV)) was performed to determine the actual shape, size, and crystal structures of GQDs, UiO-66-NH$_2$, and luminescent GQDs@UiO-66-NH$_2$ nanoprobe.

Sensing of quercetin

A highly fluorescent GQDs@UiO-66-NH$_2$ nanoprobe was employed to assess quercetin with vast sensitivity. First, 100 μg/mL previously prepared GQDs@UiO-66-NH$_2$ nanoprobe was subjected to fluorescence measurement. Then, different concentrations of 50–500 ng/mL of quercetin were individually prepared using phosphate buffer (pH = 7.4, 10 mmol/L) in cleaned 5-mL volumetric flasks. For the sensing investigation, produced quercetin concentrations were digested with the GQDs@UiO-66-NH$_2$ nanoprobe for 15 min to enable the reactivity of the GQDs@UiO-66-NH$_2$ nanoprobe. After that, the quenched fluorescence of the prepared GQDs@UiO-66-NH$_2$ nanoprobe was measured via a spectrofluorometer. The linear concentration and range and limit of detection (LOD) for quercetin were measured. Herein, ΔF was calculated using the ratio of fluorescent intensity of the probe in the non-attendance (F_0) and attendance (F) of quercetin concentrations. After that, LOD was assessed via slope (m) and standard deviation (σ), and the limit of quantification (LOQ) was measured:

$$LOD = \frac{\sigma}{m} \times 3.3 \tag{1}$$

$$LOQ = \frac{\sigma}{m} \times 10 \tag{2}$$

Other analytical parameters

To confirm the selectivity aptitude of constructed GQDs@UiO-66-NH$_2$ nanoprobe for quercetin, several metal ions, amino acids, and proteins were preferred as interfering agents mainly glucose, sodium chloride, potassium chloride, bovine serum albumin, lysine, and quercetin. In brief, the same concentration of each interfering substance and quercetin were prepared in a separate volumetric flask (5 mL) using phosphate buffer (pH = 7.4). For investigation, 5 mL of GQDs@UiO-66-NH$_2$ nanoprobe solution (100 μg/mL) was added into a separate test tube and then 1 mL of individual interfering substance was added (200 ng/mL). After that, this solution was allocated for 5 min to enable the association between the nanoprobes and interfering material. The fluorescence intensity of the GQDs@UiO-66-NH$_2$ nanoprobe was then evaluated, and the same tests were carried out for all interfering compounds and quercetin. In addition, a mixture of all interfering substances (sample Q) with quercetin was crosschecked to investigate the combined effect on the fluorescence potential of the fabricated nanoprobe. In addition, other essential parameters including precision, stability, and repeatability were measured to confirm the practical applicability of the designed fluorescent sensor.

Results and Discussion

Characterizations of GQDs, UiO-66-NH$_2$, and GQDs@UiO-66-NH$_2$ nanoprobe

UV–Vis spectroscopy

The UV–Vis absorption spectra of GQDs, UiO-66-NH$_2$, and GQDs@UiO-66-NH$_2$ nanoprobe are displayed in Fig. 3. In essence, the UV–Vis spectra of the obtained GQDs solution demonstrated a high absorption point at 276 nm that ascribed to the $\pi \rightarrow \pi^*$ transition (C＝C bond). In addition, a shoulder point at 340 nm is ascribed to n→π* transition (C＝O bond). Hence, it departs GQDs from carbon dots (CDs) [32]. As a result, it assured the effective manufacturing of GQDs from organic substrates. The UV–Vis absorption spectra of UiO-66-NH$_2$ featured

two absorption maxima, one at 273 nm and the other at approximately 365 nm. The first peak point at 273 nm corresponds to ligand-to-metal charge transfer (LMCT). The second peak spike at 365 nm is attributable to the interactions of amino groups containing lone pairs of electrons with the benzene ring's π^* orbital [33]. Furthermore, the absorption band of GQDs@UiO-66-NH$_2$ conjugate displayed a wide absorption peak at the center of 340 nm and an absorption sort of 300–500 nm, showing the combined absorption (overlapping) of GQDs and UiO-66-NH$_2$. Therefore, it assured the synthesis of GQDs and UiO-66-NH$_2$-mediated GQDs@UiO-66-NH$_2$ nanoprobe.
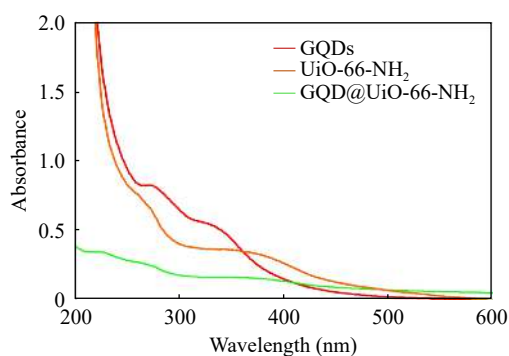

Fig. 3 UV–Vis absorption profiles of GQDs, UiO-66-NH$_2$, and GQDs@UiO-66-NH$_2$ nanoprobe.

UV cabinet fluorescence study

After proof of UV–Vis spectroscopy, the fluorescent analysis was confirmed using a UV cabinet. Figure 4 demonstrated the UV cabinet-based analysis of GQDs, obtained UiO-66-NH$_2$, and GQDs@UiO-66-NH$_2$ nanoprobe at different wavelengths. After completion of the hydrothermal reaction, the color of the precursor powder suspension changed from yellowish-brown to dark brown, which marked the green synthesis of GQDs. Herein, GQDs were observed in a laboratory UV cabinet (Fig. 4(a)) that shows yellowish-brown in visible light whereas green fluorescence (Fig. 4(b)) under λ_{max} = 254 nm light and bright blue fluorescence under UV light λ_{max} = 365 nm (Fig. 4(c)). Consequently, green synthesized GQDs had strong blue fluorescence in longer UV wavelengths which may be because of electronic energy transition [34]. Overall, it confirmed the accomplishment of GQDs from a green precursor. For UiO-66-NH$_2$, fluorescence ability was assessed in a laboratory UV cabinet. Figure 4 furnishes creamish white in visible light (Fig. 4(d)) while white fluorescence (Fig. 4(e)) under λ_{max} = 254 nm light and

bright blue fluorescence under UV light λ_{max} = 365 nm (Fig. 4(f)). As a result, it confirmed that UiO-66-NH$_2$ had strong blue fluorescence in longer UV wavelengths which may be because of 2-aminoterephthalic acid as a linker having fluorescence properties [33]. In addition, the GQDs@UiO-66-NH$_2$ nanoprobe was subjected to fluorescence study using the laboratory UV cabinet (Fig. 4). It shows creamy white in visible light (Fig. 4(g)) whereas white fluorescence (Fig. 4(h)) under λ_{max} = 254 nm light and bright blue fluorescence under UV light λ_{max} = 365 nm (Fig. 4(i)). As a result, it confirmed that UiO-66-NH$_2$ had strong blue fluorescence in longer UV wavelengths than bare UiO-66-NH$_2$ and GQDs. It's probable that the elevation in conjugate fluorescence is attributable to the fluorescence of GQDs and UiO-66-NH$_2$ (synergistic effect takes place).

Excitation and emission spectrum of GQDs

The optical characteristics of green synthesized GQDs were investigated using fluorescence excitation and emission spectroscopy in this work. Figure 5 shows the GQD fluorescence excitation and emission spectra, showing clear excitation peaks at

Fig. 4 Presentation of GQDs, UiO-66-NH$_2$, and GQDs@UiO-66-NH$_2$ nanoprobe photographs.

345 nm and emission peaks around 455 nm, respectively [35].

Particle size analysis

The particle size analysis of GQDs, UiO-66-NH$_2$, and GQDs@UiO-66-NH$_2$ is illustrated in Fig. 6. It has been asserted that particle size has the greatest consequence on optical qualities and surface stability [36]. Green-produced GQDs had a particle size of 43.5 nm (Fig. 6(a)), confirming the generation of nanosized GQDs from cornhusk. The polydispersity index (PDI) of green synthesized GQDs was determined to be 0.145, indicating that GQDs in solution is distributed uniformly. The mean particle size of UiO-66-NH$_2$ was measured to be 58.8 nm (Fig. 6(b)), and the PDI was 0.319, indicating homogeneous nanosize particle distributions in formed dispersion. The averaged particle size of the intensely fluorescent GQD@UiO-66-NH$_2$ nanoprobe was 89.4 nm (Fig. 6(c)), and the polydispersity index was 0.167, confirming homogeneous conjugate distributions. The enhancement in the size of the nanoprobe could be because of the incorporation of MOFs and GQDs. The HR-TEM study of GQD, UiO-66-NH$_2$, and GQD@UiO-66-NH$_2$ nanoprobe were undertaken for additional confirmation.

Zeta potential analysis

The zeta potential is a significant parameter that affects a solution's stability. In this line, the literature survey reported that particles having a higher positive or negative zeta potential are thought to produce a stable solution [37]. The surface charge of green-produced GQDs was –27.29 mV, revealing that GQDs are durable in solution (Fig. 7(a)). Moreover, the negative zeta of GQDs assured oxygen-based surface functionality such as hydroxyl, carboxyl, and
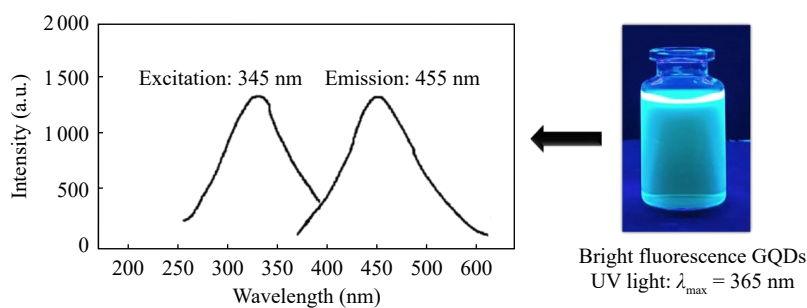

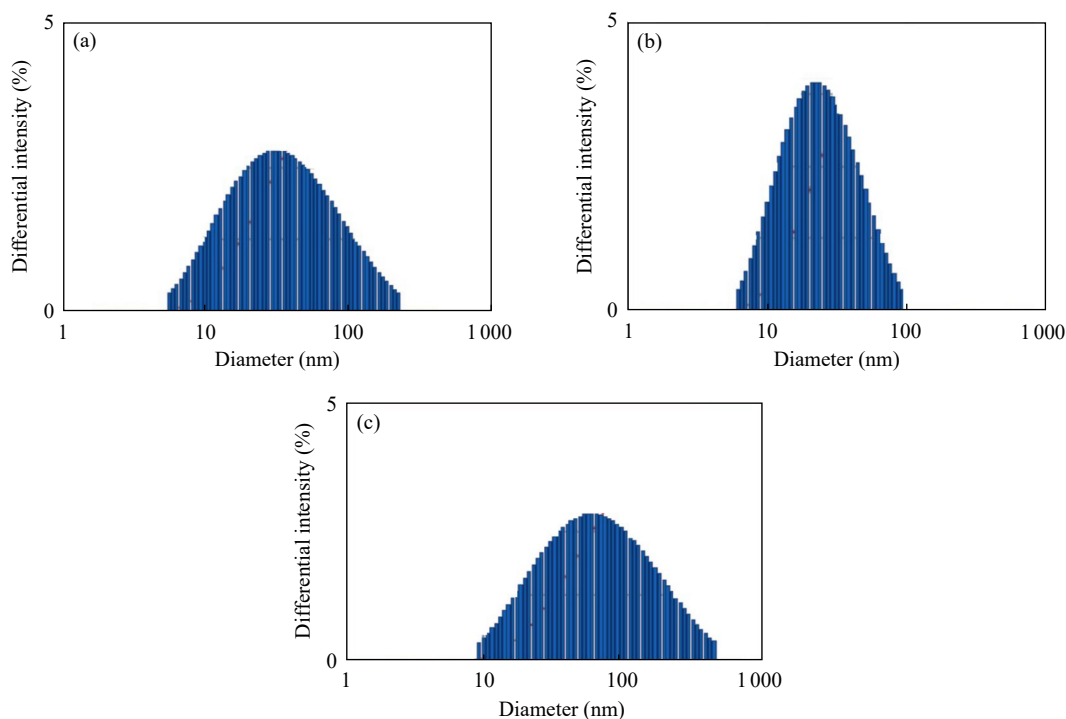**Fig. 5** Excitation and emission of green synthesized GQDs using a spectrofluorometer.

Fig. 6 Particle size analysis of (**a**) green synthesized GQDs, (**b**) bare UiO-66-NH$_2$, and (**c**) final GQDs@UiO-66-NH$_2$ nanoprobe.

epoxy [38]. The surface charge of UiO-66-NH$_2$ was observed to be +30.02 mV, which assured the stability of MOF in the solution (Fig. 7(b)). It shows the potential that may be because of the amine group on the UiO-66-NH$_2$ MOFs surface [39]. Finally, the surface charge of the fabricated GQD@UiO-66-NH$_2$ nanoprobe was +24.75 mV, which assured the good stability of the nanoprobe in the solution (Fig. 7(c)). Herein, there is a change in the zeta potential of nanoprobe as compared to the bare UiO-66-NH$_2$ MOFs and GQDs, which may be because of the conjugation/masking of surface functionality of GQDs into porous UiO-66-NH$_2$.

FTIR spectroscopy

In this step, the FTIR spectroscopy verified the hydrophilicity of green synthesise GQDs (Fig. 8(a)). In summary, O—H stretching vibration, C—H stretching vibration, C═O stretching vibration, and C—O stretching vibration were discovered to be at 3 313, 2 939, 1 638, and 1 030 cm^{-1}, respectively. Consequently, the existence of carboxylic functionality on the exterior of green-produced GQDs was verified. Figure 8(b) demonstrated the FTIR spectra of fluorescent UiO-66-NH$_2$. Briefly, peaks at 3 356 and 3 259 cm^{-1} confirmed the occurrence of amine (N—H) stretching. Herein, the overlapping of primary amines of UiO-66-NH$_2$ and OH of water molecules present in the powder of UiO-66-NH$_2$ resulted in a wide peak between the regions of 3 250–3 380 cm^{-1}. The strong intense peak point at 1 590 cm^{-1} indicated the presence of C═O stretching. The intense peak at 1 239 cm^{-1} confirmed the occurrence of C—N functionality. In addition, C—O stretching vibrations were obtained at 1 375 cm^{-1} [40]. Simply put, it validated the fabrication of UiO-66-NH$_2$ MOFs employing the recommended linker and metal ion origin. Figure 8(c) displayed FTIR of prepared luminescent GQDs@UiO-66-NH$_2$ nanoprobe. In this, different UiO-66-NH$_2$ MOFs peaks include main Zr—O stretching vibration, and symmetric/asymmetric N—H stretching vibration were observed around 400–650 and 3 356–3 259 cm^{-1}, respectively. Also, the bonding between aromatic carbon and nitrogen (C—N) was seen at 1 239 cm^{-1}. Moreover, the UiO-66-NH$_2$ —MOFs demonstrate carboxylic stretching vibrations at 1 590 cm^{-1} whereas other FTIR peaks including C—O stretching vibrations, and chloride stretching vibrations were obtained at 1 018 and 636 cm^{-1}, respectively. The FTIR peaks of —OH and —NH$_2$ were obtained at 3 050–3 600 cm^{-1} that assured the presence of primary amine in GQDs@UiO-66-NH$_2$-MOFs. In addition, a broad FTIR peak at 3 100–3 500 cm^{-1} indicates the existence of water molecules in porous 3 050–3 600 cm^{-1} (Zr—OH). Finally, the FTIR peak shifts reported the existence of hydrogen bonds across the main amine and hydroxyl units. Furthermore, certain GQDs typical spikes at around 2 900 cm^{-1} have emerged. It guaranteed the fabrication of GQDs@ UiO-66-NH$_2$ MOFs derived nanoprobes from naked GQDs and UiO-66-NH$_2$ MOFs [41].

HR-TEM analysis

The morphology and size of prepared nanosized GQDs, bare UiO-66-NH$_2$, and GQDs@UiO-66-NH$_2$ nanoprobe were confirmed using HR-TEM. Figure 9(a) depicts the HR-TEM image of green synthesized GQDs wherein it shows the uniform size distribution with 20 nm in an average diameter. Overall, it assures the synthesis of nanosize and uniform distribution of GQDs from green precursors. Figure 9(b) depicts the HR-TEM image of UiO-66-NH$_2$. It shows the regular octahedron nanostructure with 100 nm of average particle size [27]. Figure 9(c) depicts the HR-TEM image of the final GQDs@UiO-66-NH$_2$ probe. It shows the successful encapsulation of GQDs into UiO-66-NH$_2$. That may be because of the porous nature of MOFs and weak interactions with the NH$_2$ functionality of UiO-66-NH$_2$ and the carboxyl functionality of GQDs. As a result, it demonstrated that the average particle size of 10 nm confirmed that slight disruption of the structure of MOFs may be an encapsulation of GQDs in the pores of MOFs. To summarise, the GQDs@UiO-66-NH$_2$ probe was prepared utilizing green-generated GQDs and UiO-66-NH$_2$.

Sensing of quercetin

In this step, the optimization of a suitable concentration of synthesized UiO-66-NH$_2$ was accomplished using numerous concentrations with green synthesized GQDs. Herein, the addition of prepared concentration of MOFs into GQDs shows the boosting of fluorescence intensity of conjugate. Herein, the concentration of MOFs shows a proportional relationship with fluorescent intensity augmentation. Finally, 140 μg/mL UiO-66-NH$_2$ was obtained as a suitable concentration for fabrication of GQDs@UiO-66-NH$_2$ based fluorescence nanoprobe for detection of quercetin. After the addition of other
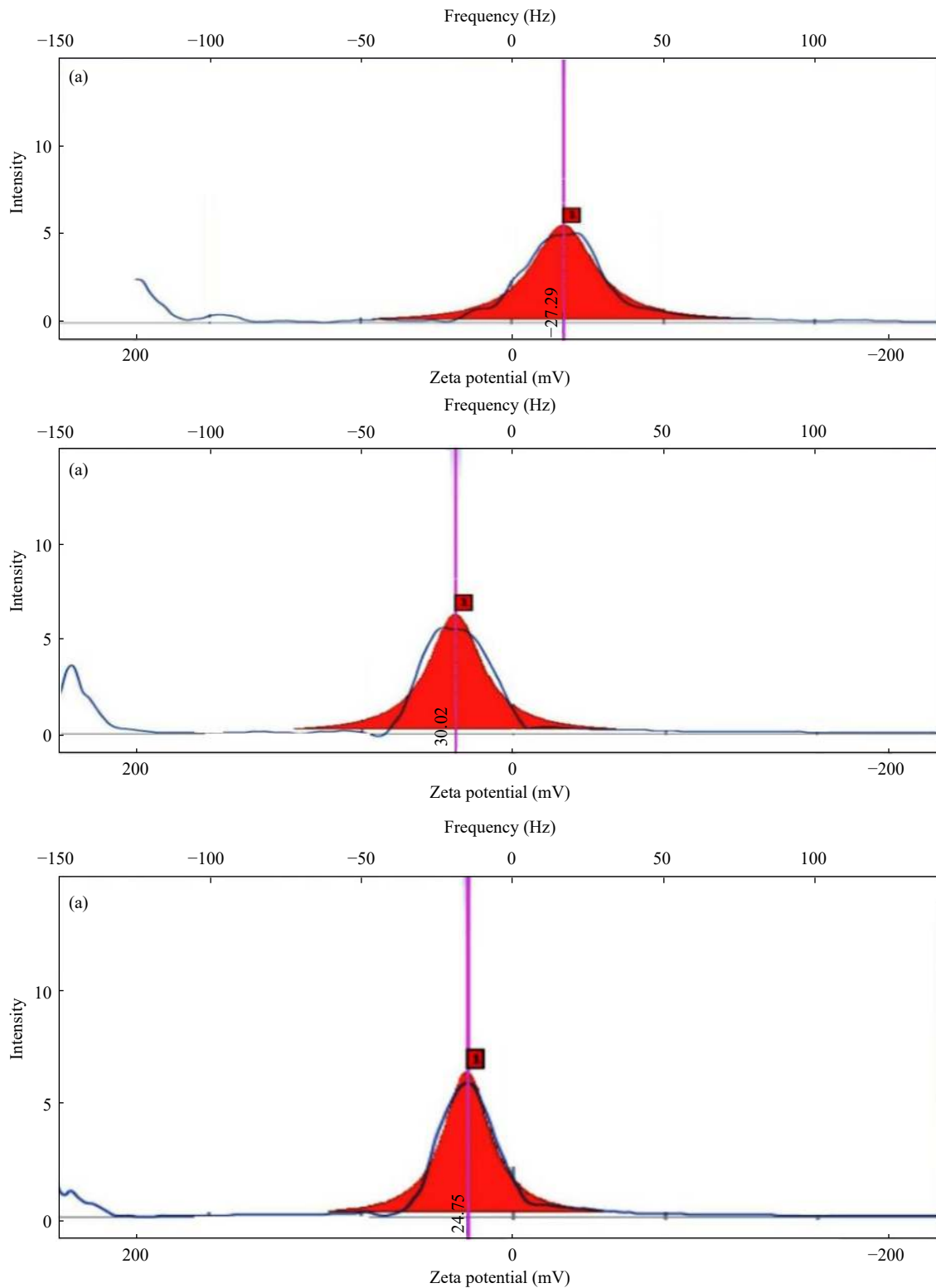
Fig. 7 Zeta potential of (**a**) green synthesized GQDs, (**b**) bare UiO-66-NH$_2$, and (**c**) final GQDs@UiO-66-NH$_2$ nanoprobe.

next concentrations, it does not demonstrate the proportional relationship which may be because of the complete conjugation of GQDs with bare UiO-66-NH$_2$. It produced more fluorescence intensity over naked GQDs and UiO-66-NH$_2$. The optimized concentration-based GQDs@UiO-66-NH$_2$ probe was further subjected to the sensing study of quercetin. In

this study, sensing of quercetin using a fabricated GQDs@UiO-66-NH$_2$ probe was depicted in Fig. 10. The addition of varied prepared quantities of quercetin culminated in the dampening of the nanoprobe's fluorescence referred to as fluorescence "Turn-Off". Herein, conjugation of GQDs and UiO-66-NH$_2$ probe resulted in the high bright blue
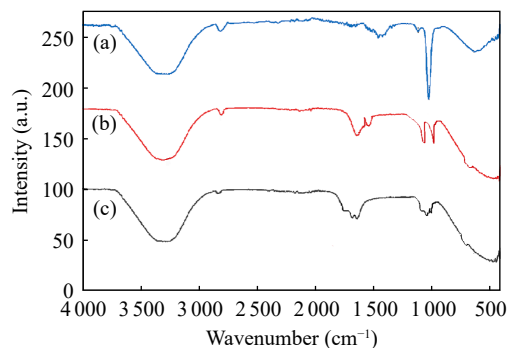
Fig. 8 FTIR spectrum of (**a**) GQDs, (**b**) bare UiO-66-NH$_2$, and (**c**) GQDs@UiO-66-NH$_2$ nanoprobe.

fluorescence. In addition, it has been divulged that the photosensitivity of UiO-66-NH$_2$ was boosted with the conjugation of green synthesized GQDs [31]. After the addition of quercetin from 50 to 500 ng/mL, it illustrates the fluorescence quenching (Fig. 10(a)). It might be due to UiO-66-NH$_2$ having a higher binding affinity and adsorption potential for quercetin. Possibly, it is because of the complexation of zirconium ions with 3-OH and 4-C═O functionality of quercetin. The calibration curve of quercetin using GQDs@UiO-66-NH$_2$ nanoprobe was provided in Fig. 10(b) ($Y = 0.0011X + 1.0395$ and $R^2 = 0.968$). As a consequence, the linear concentration range and LOD were determined to be 50–500 ng/mL and 2.82 ng/mL, accordingly. Therefore, sensing of quercetin using highly fluorescent GQDs@UiO-66-NH$_2$ nanoprobe confirmed the high sensitivity towards quercetin. Moreover, the LOQ was 8.57 ng/mL. Consequently, the developed approach's LOQ and LOD were quite low. It is attributable to the pore architecture and large surface area of MOF-based nanomaterials. In this case, loading GQDs with MOFs may also help to prevent GQDs aggregation. In addition, GQDs assist to maintain the stability of the framework of UiO-66-NH$_2$. According to a literature

review, MOFs provide selective analyte adsorption, which results in increased sensitivity and selectivity. Herein, the addition of quercetin resulted in the fluorescence quenching of GQDs@UiO-66-NH$_2$ nanoprobe with a directly proportional relationship. Possibly, it may be because of static plus dynamic fluorescence quenching tactics whereas literature reported that the immunofixation (IFE), photo-induced electron transfer (PET), and Förster resonance energy transfer (FRET) as a fluorescent quenching process. In FRET, it involved energy relocation from a donor site (excited state) to an acceptor site (ground state) via dipole–dipole interaction. In addition, owing to a porous framework of UiO-66-NH$_2$ in a nanoprobe offers a boosted sensitivity towards quercetin [42].

Anti-interference potential of GQDs@UiO-66-NH$_2$ nanoprobe

The anti-interference aptitude of fabricated GQDs@UiO-66-NH$_2$ nanoprobe was measured using a different interfering agent. The fluorescence intensity of the produced fluorescent nanoprobe was reduced by a minor amount in the presence of other chosen interfering chemicals. Importantly, it might be because UiO-66-NH$_2$ has a higher binding affinity and adsorption capability for quercetin than the other interfering agents. Furthermore, a combination of all interfering compounds quenched the fluorescence of the nanoprobe slightly more than pure quercetin in the nanoprobe. Overall, it confirmed the anti-interference potential of GQDs@UiO-66-NH$_2$ nanoprobe towards the quercetin in the occurrence of several biomolecules and ions. After this, GQDs@UiO-66-NH$_2$ precision was reported here based on interday ($n = 6$) and intraday ($n = 6$) output. In consequence, the relative standard deviation (RSD) was determined
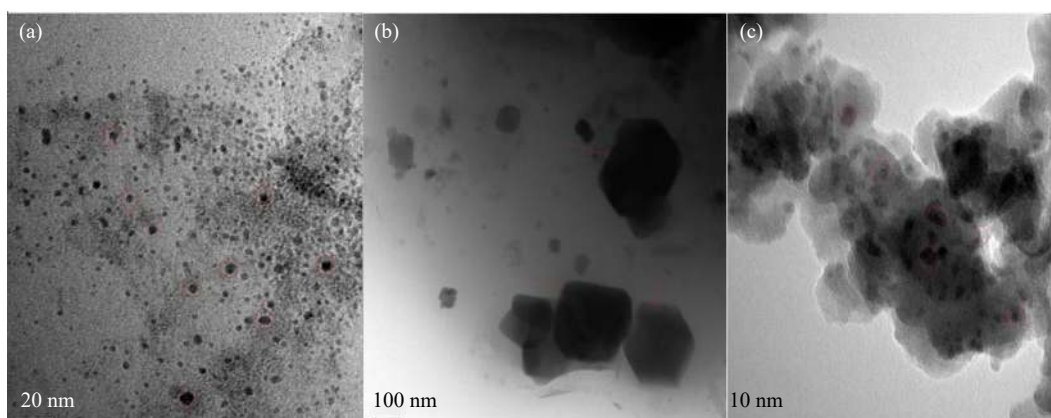

Fig. 9 HR-TEM images of (**a**) GQDs, (**b**) bare UiO-66-NH$_2$, and (**c**) GQDs@UiO-66-NH$_2$ probe.
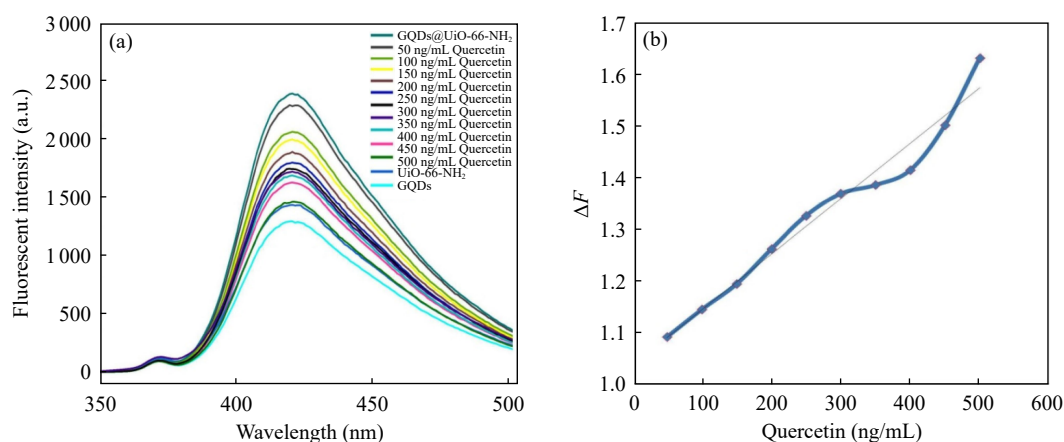
Fig. 10 (a) Sensing of quercetin using nanosize GQDs@UiO-66-NH$_2$ probe. **(b)** Calibration curve of concentration of quercetin (50–500 ng/mL) vs. fluorescence quenching efficiency (ΔF)

to be 1.20% for interday and 3.56% for intraday, respectively. The repeatability of the projected final GQDs@UiO-66-NH$_2$ nanosized sensor was then determined using 300 ng/mL of quercetin, resulting in RSD of 2.90% (less than 5%). It ensured that the suggested sensor for measuring quercetin is repeatable. Finally, the suggested sensor's stability was tested for 10 days at 25 °C. The RSD was determined to be 4.20% (less than 5%), indicating that the sensor is stable for up to 10 days under testing circumstances.

Conclusion

The present work reported the GQDs@UiO-66-NH$_2$-based fluorescence "Turn-On–Off" nanoprobe for the detection of quercetin. In conclusion, nanosize stable GQDs were obtained from corn husk whereas UiO-66-NH$_2$ was synthesized using 2-ATA as an organic linker and zirconium as a metal ions source via the hydrothermal method. The significant increment in fluorescence of nanoprobe to the bare GQDs and UiO-66-NH$_2$ assured the synthesis of a high fluorescent sensor. The UV–Vis spectroscopy confirmed the formation GQDs, UiO-66-NH$_2$, and GQDs@UiO-66-NH$_2$. The zeta potential of GQDs, UiO-66-NH$_2$, and GQDs@UiO-66-NH$_2$ assured the stability of the prepared nanoprobe. The HR-TEM images signify the distribution of GQDs in the porous structure of UiO-66-NH$_2$ without any structural collapse. Finally, the sensing study shows that the addition of quercetin into the nanoprobe shows the quenching of bright fluorescent and provides a wide concentration range. Herein, owing to the towering affinity of porous UiO-66-NH$_2$, it shows the response to quercetin. Probably, the complexation of zirconium ions with 3-OH and

4-C$=$O functionality of quercetin may responsible for decrease in fluorescence intensity. The further analytical features including stability, repeatability, selectivity, and precision assured the development of an ideal sensor for the detection of quercetin. Overall, this nanosize design of fluorescence-based GQDs@UiO-66-NH$_2$ nanoprobe can be used as an outstanding alternative for sensing quercetin in biological samples and other various analytical purposes owing to their facile, speedy, cost-effective, eco-friendly, highly sensitive, and selective sensing ability.

CRediT Author Statement

Sopan Nangare: Conceptualization, investigation, methodology, project administration, supervision, visualization, writing (original draft), review, and editing. **Sayali Patil:** Data curation, writing, review, and editing. **Kalyani Chaudhari:** Data curation, writing, review, and editing. **Zamir Khan:** Data curation, writing, review, and editing. **Ashwini Patil:** Data curation, writing, review, and editing. **Pravin Patil:** Conceptualization, investigation, methodology, project administration, supervision, visualization, writing (original draft), review, and editing.

Conflict of Interest

The authors declare no competing interest exists.

References

[1] K. Ishii, T. Furuta, Y. Kasuya. High-performance liquid chromatographic determination of quercetin in human

plasma and urine utilizing solid-phase extraction and ultraviolet detection. *Journal of Chromatography B*, 2003, 794: 49−56. https://doi.org/10.1016/s1570-0232(03)00398-2

[2]   L. Durai, C. Y. Kong, S. Badhulika. One-step solvothermal synthesis of nanoflake-nanorod WS_2 hybrid for non-enzymatic detection of uric acid and quercetin in blood serum. *Materials Science and Engineering: C*, 2020, 107: 110217. https://doi.org/10.1016/j.msec.2019.110217

[3]   X. Kan, T. Zhang, M. Zhong, et al. CD/AuNPs/MWCNTs based electrochemical sensor for quercetin dual-signal detection. *Biosensors and Bioelectronics*, 2016, 77: 638−643. https://doi.org/10.1016/j.bios.2015.10.033

[4]   X. Chen, Q. Li, S. Yu, et al. Activated silica gel based carbon paste electrodes exhibit signal enhancement for quercetin. *Electrochimica Acta*, 2012, 81: 106−111. https://doi.org/10.1016/j.electacta.2012.07.063

[5]   H. Lian, Y. Kang, S. Bi, et al. Direct determination of trace aluminum with quercetin by reversed-phase high performance liquid chromatography. *Talanta*, 2004, 62: 43−50. https://doi.org/10.1016/S0039-9140(03)00405-3

[6]   J. Wittig, M. Herderich, E. U. Graefe, et al. Identification of quercetin glucuronides in human plasma by high-performance liquid chromatography–tandem mass spectrometry. *Journal of Chromatography B: Biomedical Sciences and Applications*, 2001, 753: 237−243. https://doi.org/10.1016/S0378-4347(00)00549-1

[7]   G.R. Xu, S. Kim. Selective determination of quercetin using carbon nanotube-modified electrodes. *Electroanalysis: An International Journal Devoted to Fundamental and Practical Aspects of Electroanalysis*, 2006, 18: 1786−1792. https://doi.org/10.1002/elan.200603587

[8]   G. Chen, H. Zhang, J. Ye. Determination of rutin and quercetin in plants by capillary electrophoresis with electrochemical detection. *Analytica Chimica Acta*, 2000, 423: 69−76. https://doi.org/10.1016/S0003-2670(00)01099-0

[9]   M. Veerapandian, Y.T. Seo, K. Yun, et al. Graphene oxide functionalized with silver@silica–polyethylene glycol hybrid nanoparticles for direct electrochemical detection of quercetin. *Biosensors and Bioelectronics*, 2014, 58: 200−204. https://doi.org/10.1016/j.bios.2014.02.062

[10]   N.H. Khand, A.R. Solangi, S. Ameen, et al. A new electrochemical method for the detection of quercetin in onion, honey and green tea using Co_3O_4 modified GCE. *Journal of Food Measurement and Characterization*, 2021, 15: 3720−3730. https://doi.org/10.1007/s11694-021-00956-0

[11]   M. Vinitha, K. Naveen, S.M. Chen, et al. Electrochemical determination of quercetin using glassy carbon electrode modified with $WS_2/GdCoO_3$ nanocomposite. *Mikrochim Acta*, 2022, 189: 118. https://doi.org/10.1007/s00604-022-05219-3

[12]   S.N. Nangare, P.O. Patil. Affinity-based nanoarchitectured biotransducer for sensitivity enhancement of surface plasmon resonance sensors for *in vitro* diagnosis: A review. *ACS Biomaterials Science & Engineering*, 2020, 7: 2−30. https://doi.org/10.1021/acsbiomaterials.0c01203

[13]   S. Kadian, G. Manik. Sulfur doped graphene quantum dots as a potential sensitive fluorescent probe for the detection of quercetin. *Food Chemistry*, 2020, 317: 126457. https://doi.org/10.1016/j.foodchem.2020.126457

[14]   J.H. Jin, C. Kwon, W. Park, et al. Electrochemical characterization of a glassy carbon electrode modified with microbial succinoglycan monomers and multi-wall carbon nanotubes for the detection of quercetin in an aqueous electrolyte. *Journal of Electroanalytical Chemistry*, 2008, 623: 142−146. https://doi.org/10.1016/j.jelechem.2008.07.002

[15]   S. Nangare, S. Baviskar, A. Patil, et al. Design of "Turn-Off" fluorescent nanoprobe for highly sensitive detection of uric acid using green synthesized nitrogen-doped graphene quantum dots. *Acta Chimica Slovenica*, 2022, 69: 437−447. https://doi.org/10.17344/acsi.2022.7333

[16]   R.S. Tade, S.N. Nangare, A.G. Patil, et al. Recent advancement in bio-precursor derived graphene quantum dots: Synthesis, characterization and toxicological perspective. *Nanotechnology*, 2020, 31: 292001. https://doi.org/10.1088/1361-6528/ab803e

[17]   Y.C. Chen, W.H. Chiang, D. Kurniawan, et al. Impregnation of graphene quantum dots into a metal–organic framework to render increased electrical conductivity and activity for electrochemical sensing. *ACS Applied Materials & Interfaces*, 2019, 11: 35319−35326. https://doi.org/10.1021/acsami.9b11447

[18]   J. Pantwalawalkar, S. Chandankar, R. Tade, et al. Graphene quantum dot based ultrasensitive probe for biosensing of prostate cancer biomarkers: Current updates and future challenges. Advances in *Natural Sciences: Nanoscience and Nanotechnology*, 2022, 13: 013001. https://doi.org/10.1021/acsami.9b11447

[19]   C. Stefanov, C.C. Negut, L.A.D. Gugoasa, et al. Gold nanoparticle-graphene quantum dots nanozyme for the wide range and sensitive electrochemical determination of quercetin in plasma droplets. *Microchimica Acta*, 2020, 187: 1−10. https://doi.org/10.1007/s00604-020-04587-y

[20]   P. Zhao, M. Ni, Y. Xu, et al. A novel ultrasensitive electrochemical quercetin sensor based on MoS_2-carbon nanotube@graphene oxide nanoribbons/HS-cyclodextrin/graphene quantum dots composite film. *Sensors and Actuators B: Chemical*, 2019, 299: 126997. https://doi.org/10.1016/j.snb.2019.126997

[21]   S.N. Nangare, P.M. Sangale, A.G. Patil, et al. Surface architectured metal organic frameworks-based biosensor for ultrasensitive detection of uric acid: Recent advancement and future perspectives. *Microchemical Journal*, 2021, 169: 106567. https://doi.org/10.1016/j.microc.2021.106567

[22]   S.N. Nangare, S.R. Patil, A.G. Patil, et al. Structural design of nanosize-metal–organic framework-based sensors for detection of organophosphorus pesticides in food and water samples: Current challenges and future prospects. *Journal of Nanostructure in Chemistry*, 2022, 12: 729−764. https://doi.org/10.1007/s40097-021-00449-y

[23]   Z.G. Khan, M.R. Patil, S.N. Nangare, et al. Surface nanoarchitectured metal–organic frameworks-based sensor for reduced glutathione sensing: A review. *Journal of Nanostructure in Chemistry*, 2022, 12: 1053−1074. https://doi.org/10.1007/s40097-022-00480-7

[24]   D. Zhang, Z. Wu, X. Zong. Metal-organic frameworks-derived zinc oxide nanopolyhedra/S, N: graphene quantum dots/polyaniline ternary nanohybrid for high-performance acetone sensing. *Sensors and Actuators B: Chemical*, 2019, 288: 232−242. https://doi.org/10.1016/j.snb.2019.02.093

[25]   S.N. Nangare, A.G. Patil, S.M. Chandankar, et al. Nanostructured metal–organic framework-based luminescent sensor for chemical sensing: Current challenges and future prospects. *Journal of Nanostructure in Chemistry*, 2022, 13: 197−242. https://doi.org/10.1007/s40097-022-00479-0

[26]   S. Xie, X. Li, L. Wang, et al. High quantum-yield carbon dots embedded metal-organic frameworks for selective and sensitive detection of dopamine. *Microchemical Journal*, 2021, 160: 105718. https://doi.org/10.1016/j.microc.2020.105718

[27] L. Lu, M. Ma, C. Gao, et al. Metal organic framework@polysilsesequioxane core/shell-structured nanoplatform for drug delivery. *Pharmaceutics*, 2020, 12: 98. https://doi.org/10.3390/pharmaceutics12020098

[28] S. Nangare, S. Patil, A. Patil, et al. Bovine serum albumin-derived poly-L-glutamic acid-functionalized graphene quantum dots embedded UiO-66-NH$_2$ MOFs as a fluorescence ' On-Off-On' magic gate for para-aminohippuric acid sensing. *Journal of Photochemistry and Photobiology A*: *Chemistry*, 2023, 438: 114532. https://doi.org/10.1016/j.jphotochem.2022.114532

[29] H. Xu, S. Zhou, L. Xiao, et al. Fabrication of a nitrogen-doped graphene quantum dot from MOF-derived porous carbon and its application for highly selective fluorescence detection of Fe^{3+}. *Journal of Materials Chemistry C*, 2015, 3: 291−297. https://doi.org/10.1039/C4TC01991A

[30] H. Abdolmohammad-Zadeh, F. Ahmadian. A fluorescent biosensor based on graphene quantum dots/zirconium-based metal-organic framework nanocomposite as a peroxidase mimic for cholesterol monitoring in human serum. *Microchemical Journal*, 2021, 164: 106001. https://doi.org/10.1016/j.microc.2021.106001

[31] S. Safa, M. Khajeh, A.R. Oveisi, et al. Graphene quantum dots incorporated UiO-66-NH$_2$ as a promising photocatalyst for degradation of long-chain oleic acid. *Chemical Physics Letters*, 2021, 762: 138129. https://doi.org/10.1016/j.cplett.2020.138129

[32] S. Ahirwar, S. Mallick, D. Bahadur. Electrochemical method to prepare graphene quantum dots and graphene oxide quantum dots. *ACS Omega*, 2017, 2: 8343−8353. https://doi.org/10.1021/acsomega.7b01539

[33] Y. Hao, S. Chen, Y. Zhou, et al. Recent progress in metal–organic framework (MOF) based luminescent chemodosimeters. *Nanomaterials*, 2019, 9: 974. https://doi.org/10.3390/nano9070974

[34] P. Zheng, N. Wu. Fluorescence and sensing applications of graphene oxide and graphene quantum dots: A review. *Chemistry–An Asian Journal*, 2017, 12: 2343−2353. https://doi.org/10.1002/asia.201700814

[35] K. Saenwong, P. Nuengmatcha, P. Sricharoen, et al. GSH-doped GQDs using citric acid rich-lime oil extract for highly selective and sensitive determination and discrimination of Fe^{3+} and Fe^{2+} in the presence of H$_2$O$_2$ by a fluorescence "turn-off" sensor. *RSC Advances*, 2018, 8: 10148−10157. https://doi.org/10.1039/C7RA13432K

[36] H. Lin, C. Huang, W. Li, et al. Size dependency of nanocrystalline TiO$_2$ on its optical property and photocatalytic reactivity exemplified by 2-chlorophenol. *Applied Catalysis B*: *Environmental*, 2006, 68: 1−11. https://doi.org/10.1016/j.apcatb.2006.07.018

[37] S. Samimi, N. Maghsoudnia, R. B. Eftekhari, et al. Chapter 3—Lipid-based nanoparticles for drug delivery systems. Characterization and biology of nanomaterials for drug delivery. Elsevier, 2019: 47–76. https://doi.org/10.1016/j.apcatb.2006.07.018

[38] L.N. Dinh, L.N. Ramana, V. Agarwal, et al. Miniemulsion polymerization of styrene using carboxylated graphene quantum dots as surfactant. *Polymer Chemistry*, 2020, 11: 3217−3224. https://doi.org/10.1039/D0PY00404A

[39] A.H. Ibrahim, W.A. El-Mehalmey, R.R. Haikal, et al. Tuning the chemical environment within the UiO-66-NH$_2$ nanocages for charge-dependent contaminant uptake and selectivity. *Inorganic Chemistry*, 2019, 58: 15078−15087. https://doi.org/10.1021/acs.inorgchem.9b01611

[40] K. Tabatabaeian, M. Simayee, A. Fallah-Shojaie, et al. N-doped carbon nanodots@ UiO-66-NH$_2$ as novel nanoparticles for releasing of the bioactive drug, rosmarinic acid and fluorescence imaging. *DARU Journal of Pharmaceutical Sciences*, 2019, 27: 307−315. https://doi.org/10.1007/s40199-019-00276-1

[41] M. Bagherzadeh, A. Bayrami, M. Amini. Enhancing forward osmosis (FO) performance of polyethersulfone/polyamide (PES/PA) thin-film composite membrane via the incorporation of GQDs@UiO-66-NH$_2$ particles. *Journal of Water Process Engineering*, 2020, 33: 101107. https://doi.org/10.1016/j.jwpe.2019.101107

[42] M.K. Bera, L. Behera, S. Mohapatra. A fluorescence turn-down-up detection of Cu^{2+} and pesticide quinalphos using carbon quantum dot integrated UiO-66-NH$_2$. *Colloids and Surfaces A*: *Physicochemical and Engineering Aspects*, 2021, 624: 126792. https://doi.org/10.1016/j.colsurfa.2021.126792